Control Engineering Practice 112 (2021) 104805

Contents lists available at ScienceDirect

Control Engineering Practice

journal homepage: www.elsevier.com/locate/conengprac

Design and experimental validation of three way catalyst age estimator and Fisher information analysis for optimal sensor selection ☆

S. Gelmini [a], M.A. Hoffmann [b], S. Onori [c,*]

[a] Department of Mechanical Engineering - Massachusetts Institute of Technology, 77 Massachusetts Ave, Cambridge, MA, 02139, USA
[b] Department of Mechanical Engineering - Auburn University, 354 War Eagle Way, Auburn, AL 36849, USA
[c] Department of Energy Resources Engineering - Stanford University, Stanford, CA, 94305, USA

ARTICLE INFO

Keywords:
Three-way catalyst
Extended Kalman Filter
Fisher information analysis
Rapid control prototyping

ABSTRACT

Three way catalysts (TWCs) are installed downstream of internal combustion engines to mitigate the engine out pollutants generated from combustion. Accurate engine control systems are needed to achieve high conversion efficiency during vehicle operation and optimize TWC inputs. Accounting for TWC internal dynamics within the exhaust emission control design is key to enable improved engine and catalyst performance.

However, since internal TWC dynamics cannot be directly measured, modeling and estimation of the converter's dynamics are essential for the development of high performing exhaust emission control strategies. In this paper, a Dual Extended Kalman Filter (dEKF) is designed and experimentally validated for the estimation of both the TWC oxygen storage level, ϕ, and age-dependent oxygen storage capacity, OSC. The estimator design is based on an experimentally validated physics-based TWC model developed by the authors in a previous work. Observer validation and performance evaluation are conducted over transient drive cycles in a chassis dynamometer. Moreover, observability properties and related estimation performance are analyzed using different sensor technologies. It is found out that using switch-type oxygen sensors in place of wideband oxygen sensors leads to a loss of observability within the model, preventing real-time OSC determination and, therefore, aging estimation. A Fisher information quantity study is developed and presented that provides quantitative guidelines for the optimization of TWC sensor design. Finally, the observer is tested on real hardware via rapid control prototyping.

1. Introduction

Economic and population growth along with the rapid suburbanization experienced in the second half of the last century have led to a transport system that heavy relies on personal vehicles for transportation, (EPA - History of Reducing Air Pollution from Transportation in the United States (U.S.), 2020). Despite the efforts from regulatory agencies, like the European Environment Agency (EEA) and the Environmental Protection Agency (EPA), to impose environmental policies focused on reducing pollutant emissions from vehicles (see, for instance, Fig. 1), carbon dioxide (CO_2) emissions, the main greenhouse gas produced by the transportation sector, have steadily increased (IPPC, 2014).

Three way catalytic converters are exhaust emission control devices aimed at reducing tail-pipe emissions by catalyzing a redox (oxidation and reduction) reaction. In particular, it converts the engine out pollutants like nitrogen oxides NO_x, carbon monoxide, CO, and hydrocarbons, HC, into CO_2, N_2 and water. Catalytic converters can reach up to 100% efficiency when the normalized airfuel ratio is near stoichiometry. Normalized air fuel ratio (λ) is defined as the ratio between the actual air to fuel ratio $(A/F)_{actual}$ and the stoichiometric air fuel ratio $(A/F)_{stoich}$,

$$\lambda = \frac{(A/F)_{actual}}{(A/F)_{stoich}}, \tag{1}$$

where $(A/F)_{actual} = m_{air}/m_{fuel}$ and $(A/F)_{stoich} = 14.7$ for gasoline engines. When the $(A/F)_{actual}$ is less than stoichiometry ($\lambda < 1$), the combustion is referred to as *rich*, whereas when lambda is greater than stoichiometry ($\lambda > 1$), engine operation is referred to as *lean*. Ceria-based compounds have been used since the 1980s (Gandhi, Piken, Shelef, & Delosh, 1976) to enlarge the "operating window" of the converter, improving TWC conversion efficiency during transient engine operations by allowing the catalyst to store oxygen when operating lean, and release oxygen during rich operation (Kim, 1982).

Because the catalyst oxygen storage level cannot be measured directly, real-time estimation from available sensor measurements (such

☆ The authors conducted the research documented in this paper while they were at Clemson University.

* Corresponding author.
E-mail addresses: gelmini@mit.edu (S. Gelmini), mhoffman@auburn.edu (M.A. Hoffmann), sonori@stanford.edu (S. Onori).

https://doi.org/10.1016/j.conengprac.2021.104805
Received 23 October 2020; Received in revised form 16 March 2021; Accepted 18 March 2021
Available online xxxx
0967-0661/

Nomenclature

m_{air}	Mass of air
m_{fuel}	Mass of fuel
λ	Normalized air fuel ratio
t	Time ([s])
z	Axial dimension ([m])
T_g	Gas temperature ([K])
$\dot{m}_{exh}$	Exhaust gas mass flow rate ($\left[\frac{\text{kg}}{\text{s}}\right]$)
A_{cs}	TWC cross sectional area ($[\text{m}^2]$)
T_{cat}	TWC solid phase temperature ([K])
T_{exh}	Exhaust gas temperature ([K])
R_l	Reaction rate for the lth reaction ($\left[\frac{\text{mol}}{\text{m}^3 \cdot s}\right]$)
c_0	Total exhaust gas concentration ($\left[\frac{\text{mol}}{\text{m}^3}\right]$)
k_j^f	Forward reaction rate ($j = 1, 2$)
k_j^b	Backward reaction rate ($j = 1, 2$)
P	Exhaust gas pressure ([Pa])
R	Universal gas constant ($R = 8.314$) ($\left[\frac{\text{J}}{\text{kg} \cdot \text{K}}\right]$)
A_j	Arrhenius pre-exponential factor
E_j	Activation energy ([J])
K_j	Chemical equilibrium constant
u	Space velocity ($\left[\frac{\text{m}}{\text{s}}\right]$)
M_{exh}	Average molar mass of composition ($\left[\frac{\text{kg}}{\text{mol}}\right]$)
OSC	Oxygen storage capacity ($\left[\frac{\text{mol}}{\text{m}^3}\right]$)
ϕ	Oxygen storage level ([0 – 1])
t_s	Sampling time ([s])
j	Reaction index
i	Discrete cell index
c	Chemical species index
$[\mathcal{X}]$	Gas specie $\mathcal{X}$ concentration ($\left[\frac{\text{mol}}{\text{m}^3}\right]$)
f	Forward
b	Backward
A^T	Matrix A transposition
$F(\theta^o)$	Fisher information quantity
$Var\left(\hat{\theta}\right)$	Variance of identified parameter $\hat{\theta}$

as pre- and post-catalyst exhaust gas oxygen sensors) is key for the enhancement of the TWC operation (Balenovic, Backx, & Hoebink, 2001). In this paper, the level of oxygen in the TWC at any given time is indicated by $\phi(t)$, Sabatini et al. (2015). Modern AFR control strategies are likely to operate directly on a real-time oxygen storage estimate to increase conversion of the harmful exhaust species in the TWC. As the TWC performance degrades overtime, the oxygen storage capacity, OSC, lumps together multiple aging effects, such as thermal and chemical aging mechanisms (Cooper, 1983; González-Velasco et al., 2000; Matam et al., 2012; Moldovan, Rauch, Morrison, Gomez, & Antonia Palacios, 2003; Sabatini et al., 2016) (see Figs. 2 and 3).

Accurate estimation strategies for oxygen storage level and storage capacity in addition to sophisticated control policies to regulate the oxygen storage level at a desired value are key for ensuring the mitigation of harmful emissions species. Since the introduction of TWC (Oh & Cavendish, 1982), various mathematical models have been proposed ranging from high fidelity physics-based models (Depcik & Assanis, 2005; Montenegro & Onorati, 2009; Shamim, Shen, Sengupta, Son, & Adamczyk, 2002) to empirical models (Balenovic, 2002; Brandt, Wang, & Grizzle, 2000; Jones, Roberts, Bernard, & Jackson, 2000). High fidelity models accurately describe the chemical and thermal reactions involved in the converter. These models are unsuitable for

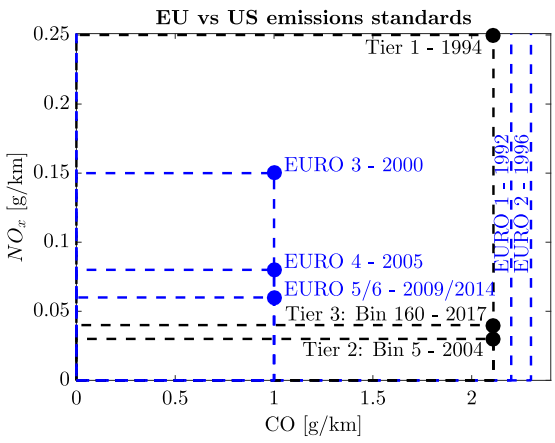

Fig. 1. History of tailpipe emission standards for the European Union and the United States (Nesbit et al., 2016). Emission targets have become more stringent over the span of the past quarter-century.

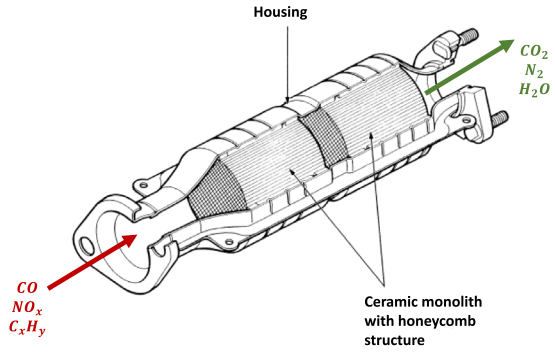

Fig. 2. Schematic of a two-brick three way catalytic device.

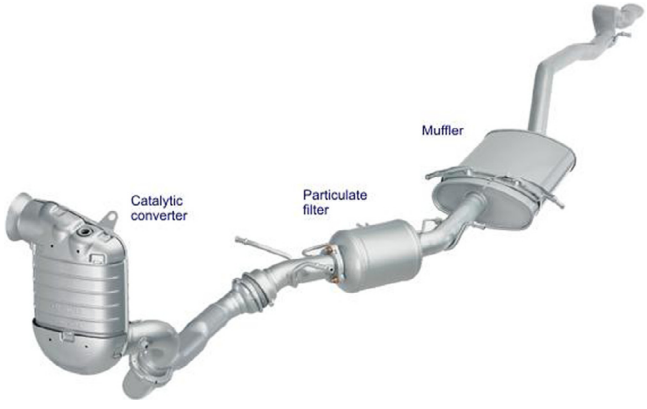

Fig. 3. Layout of a typical direct injection gasoline engine aftertreatment system. The overall architecture is composed of a three way catalytic converter, a particulate filter, and a muffler to decrease the amount of noise emitted by the exhaust of an internal combustion engine (Dieselnet website, 2020).

on-board control applications due to their high computational burden. Empirical models, on the other hand, sacrifice accuracy to gain computational efficiency. The development of emission control strategies has been widely based on empirical models (Balenovic, Backx, & de Bie, 2002; Schallock, Muske, & Jones, 2009; Tomforde, Drewelow, Duenow, Lampe, & Schultalbers, 2013), owing to their simplicity and low computational requirements. However, empirical models are heavily dependent on *ad hoc* calibration effort and large experimental data set. Moreover, when resorting to empirical models, TWC operation is

poorly predicted outside the range of operating conditions used in the calibration phase.

Reduced order modeling tools from physics-based models are designed to retain as much physics as possible while providing a computational platform compatible with the on-board requirements. In Kiwitz, Onder, and Guzzella (2012), Sabatini, Gelmini, Hoffman, and Onori (2017), model order reduction is performed by means of finite difference method (FDM) where the number of discretization nodes – each corresponding to an ordinary differential equation (ODE) – is computed by trading off computational burden and accuracy. In Godi and Onori (2017), a reduced order model for TWC temperature dynamics was developed and experimentally validated using Proper Orthogonal Decomposition (POD), and in Dettu and Onori (2021) a Galerkin-based reduction method was applied to the thermal and oxygen storage dynamics for both fresh and aged catalysts. In Santillo, Magner, Uhrich, and Jankovic (2015), by means of several simplifications applied to a complex partial-differential-equation (PDE)-based TWC model, a simple control-oriented TWC model that retained the physics of interest and was capable of real-time operation was proposed.

Reduced order models from PDE physics-based approaches are capable of capturing both the highly transient TWC dynamic behaviors of interest and their spatial characteristics. For accurate prediction and estimation of oxygen storage level and oxygen storage capacity – which are crucial for on-board diagnostics (OBD) purposes – empirical models fail to provide such a level of detail. Examples of model-based estimators using empirical models are as follows. In Ngo, Koenig, Sename, and Béchart (2013), ϕ is estimated online with a recursive least squares whereas in Muske and Jones (2004) the estimates are obtained combining the non-linear least squares with a moving-horizon estimation approach. In a recent work, Kumar, Makki, and Filev (2014), a supervised learning technique based on Support Vector Machine is used with a simple TWC dynamic model to design a diagnostic monitoring algorithm capable of distinguishing between differently aged catalysts. Meanwhile, the use of TWC physics-based models for oxygen storage estimation is found in the following contributions. In Auckenthaler, Onder, and Geering (2004), an Extended Kalman Filter (EKF) is designed to estimate ϕ and OSC using a switch-type lambda sensor downstream of the converter. However, in this work, the estimated oxygen storage is only related to the last discretization cell and not to the entire catalyst, owing to observability issues on the first cells. An EKF based on an adaptive backstepping control approach is used in Utz, Fleck, Frauhammer, Seiler-Thull, and Kugi (2014) to monitor ϕ utilizing measured TWC substrate and the inlet gas temperatures in addition to lambda switch-type sensors. However, the use of a TWC substrate temperature sensor is not a commercially viable technology. Finally, in Gelmini, Sabatini, Hoffman, and Onori (2017) a dual EKF was proposed based off post catalyst measurements from wide range lambda sensors.

Observability for nonlinear systems

In this paper, the question of whether the oxygen storage capacity, OSC, is observable, i.e. *reconstructable*, from available measurements is investigated. OSC decreases as the TWC ages. From a modeling standpoint, this can be seen as a model parameter that lumps the TWC degradation effects whose value should be tracked for diagnostics purposes. The ability to estimate OSC in real-time allows for a robust OBD capable of detecting a non-functioning TWC. In this paper, we investigate what type of measurements, *i.e.* sensor technology, would allow for on-line monitoring of TWC degradation.

In today's vehicles, the currently utilized on-board measurements within the exhaust aftertretament system are oxygen concentration and exhaust gas temperature sensors. For nonlinear TWC control dynamics, like the ones obtained in Sabatini et al. (2017) and Kiwitz et al. (2012), observability is an input-dependent property of the system (Anguelova, 2007; Hermann & Krener, 1977). If the initial system states can be uniquely determined from any measurable bounded input, then the system is said to hold the property of *uniform observability*. Since the estimation of the fast (oxygen storage level) and slow (oxygen storage capacity) TWC dynamics is required during vehicle operation, the observability analysis is extended to a given set of inputs and measurements.

Table 1
Catalyst aging specifications.

Catalyst	Aging process	Distance [1000 miles]
Green	–	0
Mid-life	Engine dyno	50
OBD	OBD aged	> 150

In this paper, the focus is on investigating whether or not the on-board sensor readings are informative enough for closed-loop estimation and control of fast and slow dynamics. Generally, when the system dynamics are not properly excited or the measurement accuracy is limited, model parameters may be identifiable only under certain input magnitudes or frequencies, or not identifiable at all. Identifiability analysis deals with the problem of parameter uniqueness when fitting a model to a set of observations. Identifiability can be exploited thanks to rigorous mathematical methods. For linear, time-invariant, differential equations, several verifiable, sufficient and necessary conditions exist (Bellman & Åström, 1970; Norton, 2009). In this paper, a Fisher information based approach is employed (Schmidt, Bitzer, Imre, & Guzzella, 2010; Sharma & Fathy, 2014; Vajda, Rabitz, Walter, & Lecourtier, 1989).

The Fisher information quantity provides a rigorous metric for assessing local parameter identifiability properties based on the likelihood function, which measures the evidence-based statistics to realize a statistical process, given in the form of measured outputs. By virtue of the Cramér–Rao's theorem, the inverse of the Fisher information quantity provides the best achievable parameter estimation covariance error, the statistical boundaries of which delimit the estimated parameter.

In this work, ϕ and OSC are estimated for differently aged catalysts with a dual EKF (dEKF), and OSC identifiability property is investigated using different sensor layouts. This research aims to provide guidance for future TWC sensor selection for robust on-board diagnostic designs.

The remainder of the paper is organized as follows. Details on the catalysts used during tests and sensor layouts are provided in Section 2. Section 3 introduces the TWC temperature and oxygen storage models and the lambda sensor technologies. Section 4 introduces Fisher information analysis used to study oxygen storage capacity identifiability properties. Section 5 describes the dEKF design and simulation results are presented in Section 6. In Section 7 results from rapid control prototyping are shown and conclusions are discussed in Section 8.

2. Problem statement and experimental set-up

The two main oxygen sensor technologies employed in the aftertreatment system are wideband and switch type lambda sensors. The goal of this work is to analyze the sensor characteristics from an observability standpoint, allowing the design of an age-dependent TWC observer and consequently, developing insights on the sensor selection aimed to monitor TWC age over its life. The capability of the two sensor technologies to retain the information needed for quantitative age estimation is quantitatively assessed.

This study utilizes TWCs of three disparate ages, namely, a Green catalyst, a Mid-Life catalyst and an OBD aged catalyst, as summarized in Table 1, Sabatini et al. (2016). The TWCs used in this work consist of a single 68 mm long monolith of 0.597 l volume.

The converters are instrumented with the following sensors:

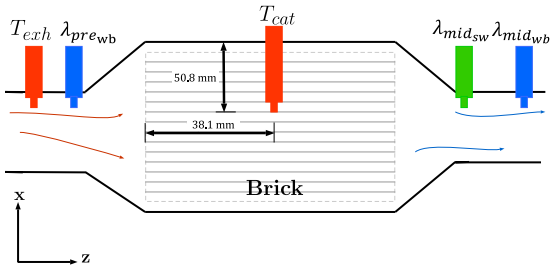

Fig. 4. A schematic of the TWC and the sensor layout used in this work. In red are the thermocouples for the exhaust inlet temperature, T_{exh}, and the mid-location catalyst temperature, T_{cat}. Wideband lambda sensors $\lambda_{pre_{wb}}$ and $\lambda_{mid_{wb}}$ are denoted in blue, while the switch-type sensor $\lambda_{mid_{sw}}$ is in green. (For interpretation of the references to color in this figure legend, the reader is referred to the web version of this article.)

- two thermocouples, one mounted upstream of the catalyst to measure the exhaust temperature, T_{exh}, and a second installed 1.5 inches from the front face of the brick and penetrating 2 inches into the flow centerline to measure the substrate temperatures, T_{cat};
- two wideband lambda sensors (Bosch LSU 4.9 with ECM F/A 1000 model controllers), located one upstream ($\lambda_{pre_{wb}}$) and one downstream ($\lambda_{mid_{wb}}$) of the catalyst;
- one switch-type lambda sensor,[1] $\lambda_{mid_{sw}}$, mounted downstream of the catalyst.

Additionally, the exhaust mass flow rate, $\dot{m}_{exh}$, used for the estimator design is obtained from the engine control unit (ECU) reading. The sensor layout schematic is shown in Fig. 4.

3. Three way catalytic converter model

A TWC is a flow-through converter that allows the exhaust gas to flow with negligible resistance and where oxidization of carbon monoxide, CO, and hydrocarbons, HC into carbon dioxide, CO_2, and water, and reduction of nitrogen oxides, NO_x, into nitrogen, take place simultaneously. Ceria and precious metals (like palladium and rhodium) are added to the surface of the cordierite substrate channels to enhance the reaction kinetics.

The conversion efficiency is dependent upon the quantity of oxygen stored in the catalyst during transient deviations of the air/fuel ratio from the stoichiometry. Oxygen storage dynamics are driven by two main reactions related to absorption/desorption of the ceria oxide, Ce_2O_3, (Bekiaris-Liberis, Jankovic, & Krstic, 2012; Sabatini et al., 2017), namely:

$$O_2 + 2 \cdot Ce_2O_3 \longleftrightarrow 2 \cdot Ce_2O_4 \tag{2a}$$

$$CO + Ce_2O_4 \longleftrightarrow CO_2 + Ce_2O_3, \tag{2b}$$

where Ce_2O_3 represents a non-oxidized ceria location, and Ce_2O_4 is an oxidized ceria site. The first reaction accounts for the oxygen adsorption on the catalyst surface whereas the second considers CO oxidation with the oxygen previously adsorbed. The rates of the two reactions described in (2a) and (2b) are:

$$R_1 = k_1^f \cdot [Ce_2O_3]^2 \cdot [O_2] - k_1^b \cdot [Ce_2O_4]^2 \cdot c_0 \tag{3a}$$

$$R_2 = k_2^f \cdot [Ce_2O_4] \cdot [CO] - k_2^b \cdot [Ce_2O_3] \cdot [CO_2], \tag{3b}$$

where $[\mathcal{X}]$ is the concentration of the chemical species $\mathcal{X}$, in $\frac{mol}{m^3}$, with $\mathcal{X} = O_2, CO, CO_2, Ce_2O_3, Ce_2O_4$. The total exhaust gas density is represented by $c_0 = \frac{P}{R \cdot T_g}$.

[1] MOPAR part 05149180AA with range 0.998 – 1.002.

Inlet gas composition is computed from the exhaust gas density as follows (Kiwitz et al., 2012):

- for stoichiometric conditions:
  - $[O_2]^* = 0.01 \cdot c_0$;
  - $[CO]^* = 0.02 \cdot c_0$;
  - $[CO_2] = 12\% \cdot c_0$.
- for conditions outside of stoichiometry:
  - $[CO] = \max\left([CO]^*, \frac{[O_2]^* + (1-\lambda)\cdot[CO_2]^*}{\lambda - \frac{1}{2}} \right)$;
  - $[O_2] = \max\left([O_2]^*, \left(\lambda - \frac{1}{2}\right) \cdot [CO]^* + (\lambda - 1) \cdot [CO_2]^* \right)$.

The forward reaction rate k_j^f (with $j = 1,2$) is a formulation of the temperature dependent Arrhenius equation, expressed as $k_j^f = A_j \cdot e^{-\frac{E_j}{R \cdot T_{cat}}}$. The backward reaction constant k_j^b (with $j = 1,2$) is evaluated as the ratio between the forward reaction rate constant and the chemical equilibrium constant K_j, thus $k_j^b = \frac{k_j^f}{K_j}$. Further details about the two reaction rates can be found in Sabatini et al. (2017).

From Shamim et al. (2002) upon simplifications made in Sabatini et al. (2017), the species concentration dynamics can be described by the following three differential equations:

$$\begin{aligned} \frac{\dot{m}_{exh}}{c_0 \cdot M_{exh} \cdot A_{cs}} \cdot \frac{\partial [O_2]}{\partial z} &= -R_1 \\ \frac{\dot{m}_{exh}}{c_0 \cdot M_{exh} \cdot A_{cs}} \cdot \frac{\partial [CO]}{\partial z} &= -R_2 \\ \frac{\dot{m}_{exh}}{c_0 \cdot M_{exh} \cdot A_{cs}} \cdot \frac{\partial [CO_2]}{\partial z} &= R_2, \end{aligned} \tag{4}$$

where the space velocity is approximated to be a function of the mass flow rate $\dot{m}_{exh}$.

The oxygen storage capacity, OSC, indicates the overall amount of oxygen that can be stored in the converter, and it is defined as the amount of oxidized and empty ceria sites in the converter:

$$OSC = [Ce_2O_3] + [Ce_2O_4]. \tag{5}$$

The oxygen storage dynamics are described as the rate of change of ϕ with respect to time, Kiwitz et al. (2012):

$$\frac{\partial \phi}{\partial t} = \frac{1}{OSC} \cdot \left(2 \cdot R_1 - R_2\right). \tag{6}$$

The overall TWC oxygen storage model was identified and validated over standard driving cycles in previous works by the authors (Sabatini et al., 2017, 2015, 2016).

A control oriented model of the TWC – in the form of Ordinary Differential Equations (ODEs) – is obtained from the PDE model via finite difference method (FDM) that divides the converter into three cells (Sabatini et al., 2017)

$$\begin{aligned} \frac{d\phi_1}{dt} &= \frac{1}{OSC} \cdot \left(2 \cdot R_1^1 - R_2^1\right) \\ \frac{d\phi_2}{dt} &= \frac{1}{OSC} \cdot \left(2 \cdot R_1^2 - R_2^2\right) \\ \frac{d\phi_3}{dt} &= \frac{1}{OSC} \cdot \left(2 \cdot R_1^3 - R_2^3\right), \end{aligned} \tag{7}$$

in which the reaction rates' superscript denote the discretization cell.

The input vector is composed of the measured air/fuel ratio upstream of the catalyst $\lambda_{pre_{wb}}$, the exhaust mass flow rate, $\dot{m}_{exh}$, and the catalyst internal temperature, T_{cat}:

$$u = \begin{bmatrix} \dot{m}_{exh} \\ T_{cat} \\ \lambda_{pre_{wb}} \end{bmatrix}, \tag{8}$$

where T_{cat} is predicted by the physics-based thermal model developed in Sabatini et al. (2015).

The output vector is defined in the next section upon the introduction of the two sensor technologies used for oxygen level sensing.

3.1. Lambda sensor technologies

During engine operation, the air/fuel ratio is controlled close to stoichiometry through the use of exhaust system feedback sensors (Heywood, 1988). The oxygen absorption/desorption from the ceria sites allows the TWC to compensate for small variations of the air-fuel ratio away from stoichiometry. Post-catalyst sensors provide quantitative information about the oxygen level to the engine to prevent either the depletion or saturation of the device.

Two different lambda sensor technologies are used today: wide band and switch-type. The wide band O_2 sensors (also known as Universal Exhaust Gas Oxygen (or UEGO) Sensors) measure the amount of oxygen in the exhaust stream, whereas the switch-type sensors – or narrow-band or Heated Exhaust Gas Oxygen (HEGO) sensors – only discriminate between rich and lean engine operation. As the system experiences an abrupt change in the oxygen content, the sensor reading is characterized by a switching behavior in the stoichiometry region.

The wide band sensor, λ_{wide}, is a function of the gas concentrations and it is modeled as follows (Kiwitz et al., 2012):

$$\lambda_{wide} = \frac{2 \cdot \left([O_2] + [CO_2]\right) + [CO]}{2 \cdot \left([CO] + [CO_2]\right)}. \tag{9}$$

On the other hand, the switch-type sensor λ_{switch} is obtained from voltage measurements using the sensor look-up table mapping the measured voltage to air/fuel ratio, $U_{\lambda_{\text{sw}}} = g(\lambda_{switch})$ as shown in Fig. 5(b).

Complex models were proposed in Auckenthaler (2005) to map, in a nonlinear fashion, the actual air-fuel ratio with the measured voltage. For control and estimation purposes, a commonly accepted model of the sensor is given by:

$$\begin{aligned} U_{\lambda_{\text{sw}}} =& E_{A,\lambda} e^{-\frac{E_{E,\lambda}}{RT_{exh}}} \log_{10}\left(1 + B_\lambda [CO]\right) \\ &- F_\lambda \log_{10}\left(1 + D_\lambda [O_2]\right) + A_\lambda, \end{aligned} \tag{10}$$

where $U_{\lambda_{\text{sw}}}$ is the measured sensor voltage (shown in Fig. 5(a)), A_λ is the sensor bias, T_{exh} is the exhaust gas temperature, [CO], [O_2] are the mole fractions of CO, O_2, and B_λ, D_λ, $E_{A,\lambda}$, $E_{E,\lambda}$, F_λ are the sensor model parameters.

Fig. 6 shows a typical air/fuel ratio signal recorded downstream of the catalyst as measured from wide band (a) and switch-type (b) lambda sensors. As shown, the signal from the switch-type is limited to a small range of values between $\mathbf{low}_{\mathbf{threshold}}$ and $\mathbf{high}_{\mathbf{threshold}}$ whose numerical values vary according to the specific sensor technology/brand used. Typical values for the $\mathbf{low}_{\mathbf{threshold}}$ and $\mathbf{high}_{\mathbf{threshold}}$ are shown in Table 2. On the other hand, the wide band sensor captures significant variations of the signal around stoichiometry.

It is worth noting that ultimately both λ_{wide} and λ_{switch} are a function of gas concentrations, which are in turn functions of OSC when the sensors are located after the TWC. In fact, both sensor models depend on the concentrations of gases that, through the reaction rate Eqs. (3) and (4) depend on the absorption and desorption of ceria oxides, which ultimately constitute the oxygen storage capacity relation (5). Such dependencies make it possible to use lambda sensors for the estimation of the aging parameter.

Although switch-type sensors are used in the post-catalyst location in commercial aftertreatment layouts, a growing interest in the use of wide band post-catalyst sensors has been seen thanks to their linear output relationship over a broader range of O_2 concentrations and lower calibration drift as a function of sensor age. These characteristics have the potential to facilitate robust control design, either via traditional proportional–integral–derivative (PID) controllers or through more sophisticated model-predictive control strategies (DE Solutions & Tecogen, 2011).

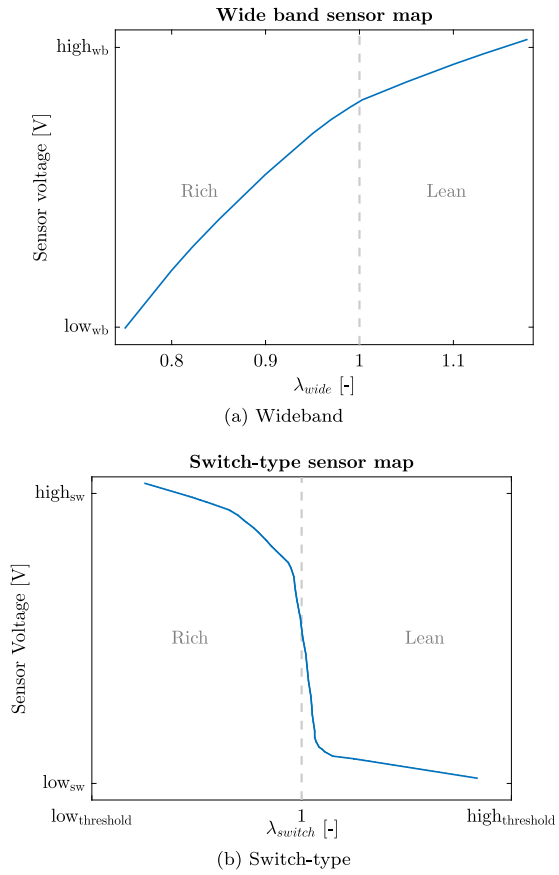

Fig. 5. (a) Wide band sensor map (Bosch, 2021) and (b) Switch-type sensor map (Mopar Part 05149180 AA datasheet, 2020) used in this work.

4. Fisher Information quantity analysis

The aim of this session is to quantitatively assess the differences between wide band and switch-type lambda sensors as it pertains to the estimation of OSC. As they carry different information about the oxygen content in the exhaust gas, the overall observability of the aging parameter $OSC = \theta$ from their respective outputs, λ_{wide} and λ_{switch_k}, is affected. In this study, the performance of wide band versus switch-type sensors is evaluated. Additionally, how switch-type sensors, in terms of their specific threshold values, are investigated for the impact of those thresholds on the state estimates. In particular, four switch-type sensors, described in Table 2, are evaluated in this study via Fisher information to construct hypothesis tests and confidence intervals using maximum likelihood estimators.

In parameter estimation theory, the Fisher information quantity is used to statistically compute the amount of information that an observable random variable carries about an unknown parameter. Over the past decade, the Fisher information quantity has been extensively used in the domain of electrochemical battery model identification as a method to select a small number of relevant experiments (or input) which are deemed sufficient to fully parametrize a model (Schmidt et al., 2010) and to estimate the accuracy of identifiable parameters (Fathy & Sharma, 2014).

In the problem under study, the output vector is defined as $y = \mathbb{R}^{5,1}$; it is also assumed measurements from $\lambda_{mid_{sw}}$ and $\lambda_{mid_{wb}}$ to be stochastic, and modeled as

$$\begin{aligned} y_i &= \lambda_{mid_{\text{sw}}} = \lambda_{switch_i} + w_{\text{sw}}, \ i = 1, \dots, 4 \\ y_5 &= \lambda_{mid_{\text{wb}}} = \lambda_{wide} + w_{\text{wb}}. \end{aligned} \tag{11}$$

The deterministic component of the signals (*i.e.*, λ_{wide} and λ_{switch}) is from the model and that corresponds to the output expected value,

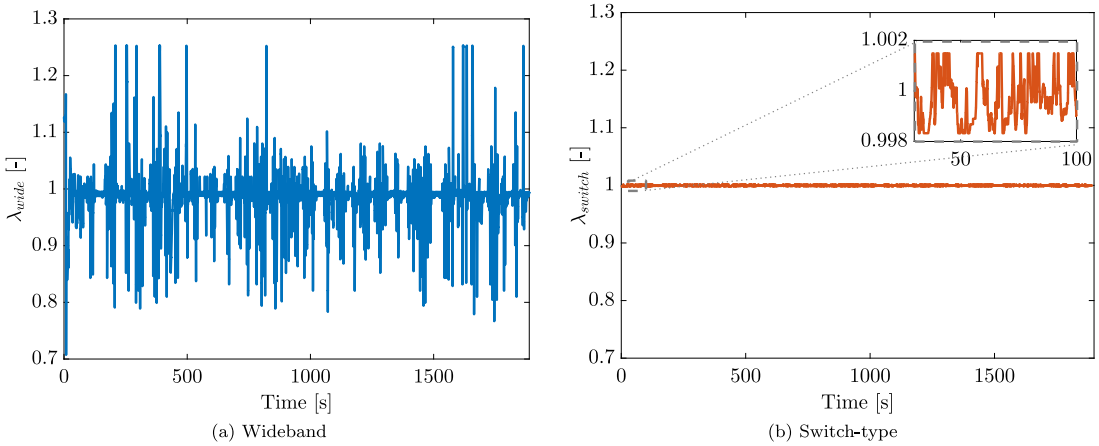

(a) Wideband (b) Switch-type

Fig. 6. Post-catalyst (a) wideband lambda sensor $\lambda_{mid_{wb}}$, and (b) switch-type lambda sensor reading, $\lambda_{mid_{sw}}$ (within the 0.998–1.002 range — as zoomed in the time interval 30 – 100 s) recorded simultaneously during the FTP driving cycle.

Table 2
Resolution of switch-type sensors depend on the low and high threshold values around stochiometry. In this work four different switch-type variants are considered.

	$Low_{threshold}$	$High_{threshold}$
$Switch_1$	0.998	1.002
$Switch_2$	0.99	1.01
$Switch_3$	0.95	1.05
$Switch_4$	0.9	1.1

whereas the superimposed noise (*i.e.*, w_{wb} and w_{wb}) is modeled through a zero-mean Gaussian random variable. More specifically, λ_{switch_k}, with $k = 1, \dots, 4$ are switch-type lambda signals characterized by different $\mathbf{low_{threshold}}$ and $\mathbf{high_{threshold}}$ values as shown in Table 2.

Therefore, the likelihood-function is defined as the probability density function of a Gaussian distribution that is a function of the measured output y_i and the parameter θ:

$$L(y_i, \theta) = \frac{1}{\sqrt{2 \cdot \pi \sigma_i^2}} e^{-\frac{\delta_i(\theta)}{2\sigma_i^2}}, \tag{12}$$

where $\delta_i(\theta) = y_i - \mu_i(\theta)$ is the difference between the lambda sensor measurements y_i as in (11), whereas $\mu_i(\theta) = \mathbb{E}\left[y_i\right]$ is the expected value of sensor y_i and is computed through the model knowing the value of θ, the unknown parameter to be estimated (*i.e.*, OSC). The Fisher information quantity is defined as the expected value of the derivative of the squared log-likelihood function with respect to the parameter θ given its optimum value

$$F(\theta^o) = \mathbb{E}\left[\frac{\partial \log L(\theta)^2}{\partial \theta}\bigg|_{\theta=\theta^o}\right]. \tag{13}$$

Expressing (13) in explicit form could be difficult as the model is nonlinear. However, (13) can be easily computed through numerical differentiation, given the optimal value of OSC for each catalyst.

The Fisher quantity is a powerful statistical tool because it provides the lower variance bound of the estimated parameter θ in the maximum-likelihood estimation (MLE) sense through the Cramér–Rao inequality

$$Var(\widehat{\theta}) \geq F(\theta^o)^{-1}. \tag{14}$$

In this study, the Fisher information quantity is used to assess how accurate the unknown parameter estimation is from the measurement of a stochastic output variable. Further details about the Fisher information quantity and, more in general, MLE can be found in Ljung (1998).

Fisher information quantity is evaluated for both the wide band lambda sensor and the four switch-type lambda sensors over different driving cycles (Federal Test Procedure (FTP), US06 and Japanese cycle JAP 15 (Dynamometer Drive Schedules, 2020), for all the available catalysts. Results of this investigation are summarized in Table 3, where the minimum variance $Var(\widehat{OSC}_{ML})$ of the MLE problem is obtained according to (14). Moreover, to quantify the loss of information in each of the four switch-type sensors relative to the wideband, the ratio of the Fisher information quantity evaluated with the wide band sensor over the different switch-type sensors is evaluated. As shown, for all the catalysts and for all the driving cycles, the wideband signal is orders of magnitude more informative than any switching sensor. This difference decreases as the admissible range of the switch-type sensors increases. This is also consistent with the results presented in Auckenthaler et al. (2004), Utz et al. (2014).

Why is this important? Employing less informative sensors in an estimation scheme leads to larger estimation uncertainties, which may not be deemed acceptable for diagnostic purposes. This is the case when detection catalyst age. In fact, a significant drop in the information contained in the sensor output introduces identifiability issues. The lack of information in the sensor signal can render it difficult (or even impossible) to obtain a reliable estimation of the unknown parameters from the available measurements. In particular, using a switch-type versus wide band lambda sensor leads to an output identifiability issue given that the available measurements used in the identification process are not informative enough to discern or unequivocally identify different parameter values in the system, *i.e* catalyst age.

The results of the Fisher analysis prove that the aging parameter, OSC, would be estimated with limited uncertainty when the estimation process is conducted using a wide band lambda sensor at the TWC brick outlet. On the other hand, when using a switch-type lambda sensor a lack of identifiability from the output is assessed, leading to higher uncertainties in the parameter identification process.

5. Dual extended kalman filter

In this section, a dEKF is presented with the goal of estimating both ϕ and OSC in real-time for robust OBD emission control design throughout the catalyst life (Fig. 7). Preliminary results of such a design were presented in Gelmini et al. (2017).

For the sake of developing a combined oxygen level and oxygen storage capacity estimator, a wide band lambda sensor is used and modeled as

$$\lambda_{mid_{\text{wb}}} = \lambda_{wide} + w_{\text{wb}}, \tag{15}$$

where w_{wb} is the sensor noise assumed to be Gaussian with zero mean and variance $R = \sigma^2_{\text{wb}}$. Its value has been estimated computing the variance of the mismatch between the measured $\lambda_{mid_{\text{wb}}}$ and its predicted counterpart (Fig. 8(b)).

Table 3
Different $\lambda_{mid_{sw}}$ sensor ranges tested for the Green, Mid-Life, and OBD catalysts.

Catalyst	Driving cycle	λ_{mid}	Fisher quantity $F(OSC^o)$	Minimum $Var\left(\widehat{OSC}\right)$	Fisher quantity ratio $\frac{switch}{wideband}$
Green	FTP	Wideband	$4.541663 \cdot 10^{-11}$	$2.201836 \cdot 10^{10}$	
		$Switch_1$	$2.870692 \cdot 10^{-20}$	$3.483480 \cdot 10^{19}$	$1.582080 \cdot 10^{9}$
		$Switch_2$	$5.553848 \cdot 10^{-18}$	$1.800553 \cdot 10^{17}$	$8.177507 \cdot 10^{6}$
		$Switch_3$	$1.427847 \cdot 10^{-15}$	$7.003551 \cdot 10^{14}$	$3.180777 \cdot 10^{4}$
		$Switch_4$	$1.863747 \cdot 10^{-14}$	$5.365535 \cdot 10^{13}$	$2.436845 \cdot 10^{3}$
	US 06	Wide band	$3.601178 \cdot 10^{-12}$	$2.776869 \cdot 10^{11}$	
		$Switch_1$	$2.785205 \cdot 10^{-20}$	$3.590400 \cdot 10^{19}$	$1.292967 \cdot 10^{8}$
		$Switch_2$	$4.741963 \cdot 10^{-18}$	$2.108831 \cdot 10^{17}$	$7.594278 \cdot 10^{5}$
		$Switch_3$	$1.546872 \cdot 10^{-15}$	$6.464660 \cdot 10^{14}$	$2.328039 \cdot 10^{3}$
		$Switch_4$	$2.493222 \cdot 10^{-14}$	$4.010874 \cdot 10^{13}$	$1.444387 \cdot 10^{2}$
	JAP 15	Wideband	$5.669884 \cdot 10^{-12}$	$1.763705 \cdot 10^{11}$	
		$Switch_1$	$2.814805 \cdot 10^{-20}$	$3.552644 \cdot 10^{19}$	$2.014308 \cdot 10^{8}$
		$Switch_2$	$3.996371 \cdot 10^{-18}$	$2.502270 \cdot 10^{17}$	$1.418758 \cdot 10^{6}$
		$Switch_3$	$1.195225 \cdot 10^{-15}$	$8.366628 \cdot 10^{14}$	$4.743781 \cdot 10^{3}$
		$Switch_4$	$1.397710 \cdot 10^{-14}$	$7.154562 \cdot 10^{13}$	$4.056554 \cdot 10^{2}$
Mid-life	FTP	Wide band	$1.889842 \cdot 10^{-13}$	$5.291448 \cdot 10^{12}$	
		$Switch_1$	$9.176624 \cdot 10^{-20}$	$1.089725 \cdot 10^{19}$	$2.059409 \cdot 10^{6}$
		$Switch_2$	$1.144978 \cdot 10^{-17}$	$8.733789 \cdot 10^{16}$	$1.650548 \cdot 10^{4}$
		$Switch_3$	$3.059139 \cdot 10^{-15}$	$3.268894 \cdot 10^{14}$	61.77692
		$Switch_4$	$2.636902 \cdot 10^{-14}$	$3.792330 \cdot 10^{13}$	7.166903
	US 06	Wide band	$6.462354 \cdot 10^{-13}$	$1.547424 \cdot 10^{12}$	
		$Switch_1$	$7.685398 \cdot 10^{-20}$	$1.301169 \cdot 10^{19}$	$8.408614 \cdot 10^{6}$
		$Switch_2$	$8.995193 \cdot 10^{-18}$	$1.111705 \cdot 10^{17}$	$7.184231 \cdot 10^{4}$
		$Switch_3$	$4.175131 \cdot 10^{-15}$	$2.395134 \cdot 10^{14}$	$1.547821 \cdot 10^{2}$
		$Switch_4$	$5.600013 \cdot 10^{-14}$	$2.472844 \cdot 10^{12}$	11.53989
	JAP 15	Wide band	$4.043927 \cdot 10^{-13}$	$2.472844 \cdot 10^{12}$	
		$Switch_1$	$8.151243 \cdot 10^{-20}$	$1.226807 \cdot 10^{19}$	$4.961117 \cdot 10^{6}$
		$Switch_2$	$7.091344 \cdot 10^{-18}$	$1.410170 \cdot 10^{17}$	$5.702624 \cdot 10^{4}$
		$Switch_3$	$2.587070 \cdot 10^{-15}$	$3.865377 \cdot 10^{14}$	$1.563130 \cdot 10^{2}$
		$Switch_4$	$2.891357 \cdot 10^{-14}$	$3.458584 \cdot 10^{13}$	13.98626
OBD	FTP	Wide band	$1.406348 \cdot 10^{-13}$	$7.110614 \cdot 10^{12}$	
		$Switch_1$	$3.450058 \cdot 10^{-19}$	$2.898502 \cdot 10^{18}$	$4.076303 \cdot 10^{5}$
		$Switch_2$	$3.395396 \cdot 10^{-17}$	$2.945164 \cdot 10^{16}$	$4.141927 \cdot 10^{3}$
		$Switch_3$	$5.424528 \cdot 10^{-15}$	$1.843478 \cdot 10^{14}$	25.92573
		$Switch_4$	$3.220330 \cdot 10^{-14}$	$3.105272 \cdot 10^{13}$	4.367094
	US 06	Wide band	$4.052825 \cdot 10^{-13}$	$2.467415 \cdot 10^{12}$	
		$Switch_1$	$1.531317 \cdot 10^{-19}$	$6.530327 \cdot 10^{18}$	$2.646627 \cdot 10^{6}$
		$Switch_2$	$2.546612 \cdot 10^{-17}$	$3.926785 \cdot 10^{16}$	$1.591457 \cdot 10^{4}$
		$Switch_3$	$6.763305 \cdot 10^{-15}$	$1.478567 \cdot 10^{14}$	59.92373
		$Switch_4$	$6.225784 \cdot 10^{-14}$	$1.606223 \cdot 10^{13}$	6.509742
	JAP 15	Wide band	$1.279241 \cdot 10^{-13}$	$7.817138 \cdot 10^{12}$	
		$Switch_1$	$1.457711 \cdot 10^{-19}$	$6.860068 \cdot 10^{18}$	$8.775678 \cdot 10^{5}$
		$Switch_2$	$3.553523 \cdot 10^{-17}$	$2.814109 \cdot 10^{16}$	$3.599922 \cdot 10^{3}$
		$Switch_3$	$4.511971 \cdot 10^{-15}$	$2.216326 \cdot 10^{14}$	28.35215
		$Switch_4$	$2.367598 \cdot 10^{-14}$	$4.223691 \cdot 10^{13}$	5.403117

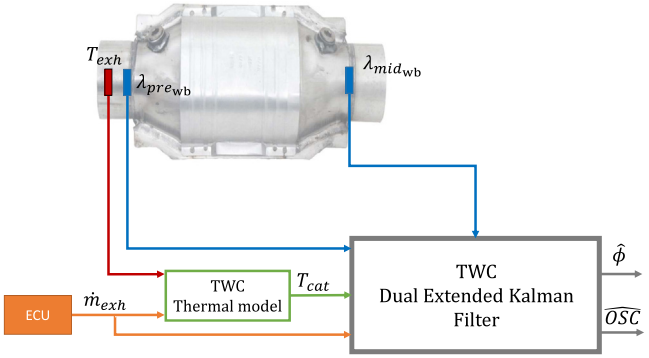

Fig. 7. Control scheme of the dEKF designed for TWC (Auto Accessories Garage, 2020). The TWC thermal model used to estimate the catalyst temperature is implemented as discussed in Sabatini et al. (2015).

The proposed dEKF is built upon a TWC model with four states. The first three states, as shown in (7), are $x_1 = \phi_1$, $x_2 = \phi_2$ and $x_3 = \phi_3$ and represent the level of oxygen storage in three different spatial locations of the TWC, whereas the fourth state is the oxygen storage capacity, $x_4 = OSC$. The overall TWC dynamics are written in a nonlinear form and discretized in the time domain using forward Euler method (Sabatini et al., 2017).

The nonlinear equations describing the ϕ dynamics are obtained from (6), whereas the rate of change of the aging state OSC is assumed to be nominally zero and subject to noise (*i.e.*, OSC is assumed to be slowly-changing variable). Model equations in the discrete time domain are therefore expressed as:

$$\begin{aligned} x_i(k+1) &= x_i(k) + T_s \cdot f_i\left(x(t), u(t)\right) + \upsilon_i, \\ &= x_i(k) + Ts \cdot \left(\frac{1}{x_4(k)} \cdot \left(2 \cdot R_1^i(k) - R_2^i(k)\right)\right) + \upsilon_i \\ x_4(k+1) &= x_4(k) + \upsilon_4 \end{aligned} \tag{16}$$

in which $i = 1, \ldots, 3$, and T_s is the sampling time, which is set to 0.01 s in this work. Instead, the predicted air/fuel ratio $\lambda_{mid_{wb}}$ is evaluated from the gas species concentrations from (9), and its discretized form

becomes:

$$y(k) = \lambda_{mid_{\text{wb}}}(k) = \lambda_{wide}(k) + w_{\text{wb}} = \frac{2 \cdot \left(\left[\text{O}_2\right](k) + \left[\text{CO}_2\right](k) \right) + \left[\text{CO}\right](k)}{2 \cdot \left(\left[\text{CO}\right](k) + \left[\text{CO}_2\right](k) \right)} + w_{\text{wb}}. \tag{17}$$

The innovation term used in the calculation of the state estimation in the EKF formulation is:

$$K(k) \cdot \left(\lambda_{mid_{\text{wb}}}(k) - \lambda_{wide}(k|k-1) \right),$$

where $K(k)$ is the Kalman gain at step k [33], $\lambda_{mid_{\text{wb}}}(k)$ is the measured air-fuel ratio, sampled at 100 Hz, and $\lambda_{wide}(k|k-1)$ is the predicted air-fuel ratio at time k computed using the states from (16) at the previous time step $k-1$.

The state-update uncertainty vector $v \in \mathbb{R}^{n_x}$ is a stochastic vector modeled as a zero mean white Gaussian noise with semi-definitive positive covariance matrix Q given as:

$$Q = diag\begin{pmatrix} Q_1 & \dots & Q_4 \end{pmatrix} = \begin{pmatrix} Q_1 & 0 & \dots & 0 \\ 0 & Q_2 & & \vdots \\ \vdots & & Q_3 & 0 \\ 0 & \dots & 0 & Q_4 \end{pmatrix}, \tag{18}$$

It is common practice to treat the elements of the covariance matrix as calibration parameters. In this case, to reduce the calibration effort, the covariance elements Q_1, Q_2, Q_3 are calculated from the mismatch generated by the high fidelity PDE TWC model (implemented with 15 cells) and the three cell model (7). In particular, x_1, x_2 and x_3 were compared from (16) with the values of oxygen storage components for cells 5, 10 and 15 in the PDE model (Sabatini et al., 2017). Fig. 8(a) shows that the process noise distributions related to the first three states of (16) is zero mean and normally distributed. The variances of such distributions are used for Q_1, Q_2, Q_3. The covariance term Q_4, related to OSC, is used as a degree of freedom for the observer calibration.

The dEKF is an extension of the Kalman filter for nonlinear systems (Grewal, 2020; Ljung, 1998; Magni & Scattolini, 2014) where the state correction and update is performed by linearizing of the nonlinear TWC dynamics at each time step. The linearization is performed numerically using the small perturbation method. For details on the observed equations, the reader is redirected to Gelmini et al. (2017).

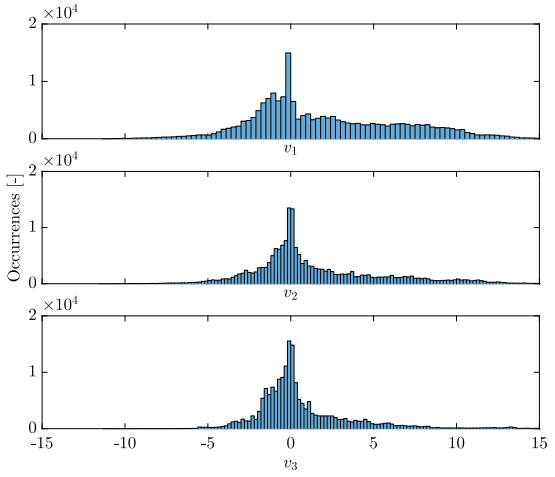

(a) Process noise distributions

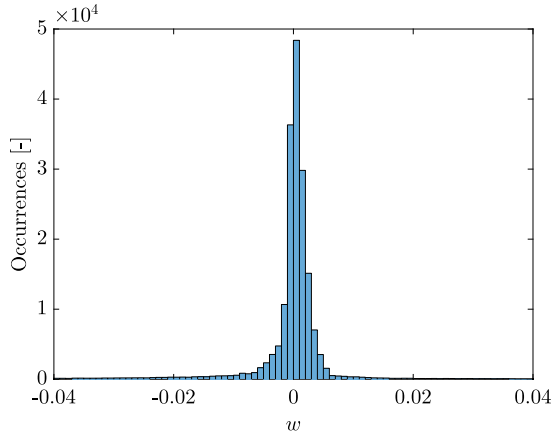

(b) Output noise distribution

Fig. 8. In (a), the process noise distributions v_i, with $i = 1, 2, 3$, evaluated over the FTP drive cycle for the Green catalyst, are shown. In (b), the output noise distribution between the real measurements $\lambda_{mid_{\text{wb}}}$ and the model output λ_{wide} is depicted.

6. Results

The objective of this work is to develop a dEKF for estimating ϕ and OSC that can be used to design a real time TWC control strategy for fuel saving and TWC health monitoring. The performance evaluation of the observer is conducted on the FTP drive cycle.

6.1. Simulation results

The performance of the dEKF is evaluated by comparing the estimated output $\hat{y}$ with the measured $\lambda_{mid_{wd}}$. Estimated ϕ and OSC are shown for all the three catalysts. The estimate of ϕ is taken as the average across the three cell state variables ϕ_i (with $i = 1, 2, 3$). Additionally, OSC estimates are normalized with respect to the value of green catalyst OSC value.

Fig. 9 shows the results of the observer design for the Green catalyst. In this case, the estimated OSC reaches its steady state value only after 1400 s. Simulations were conducted by initializing OSC to a value greater than the real one showing recovery from inaccurate initialization. The predicted output better tracks the measured $\lambda_{mid_{\text{wb}}}$ as OSC converges to the correct value.

The simulation performed with the Mid-Life catalyst (Fig. 10) shows a faster convergence, within 600 s, to the correct OSC value. More frequent deviations from stoichiometry are expected with increasing TWC age and reduced OSC. Accordingly, the estimated ϕ exhibits quicker variations relative to the Green catalyst.

Similar results are achieved for the OBD aged catalyst, as shown in Fig. 11. In this case, convergence is slower – within 1000 s – when compared to the Mid-Life device. Given that the initial OSC value is the farthest from the actual OBD value, the estimator is forced to cover the entire OSC range prior to convergence. The reduced oxygen storage buffer in the catalyst is reflected with a highly dynamic $\lambda_{mid_{wd}}$ downstream of the catalyst, resulting in pronounced ϕ variations.

The performance of the dEKF for the different catalysts is quantitatively measured in terms of output prediction accuracy via root mean square error (RMSE), defined as

$$RMSE = \sqrt{\frac{1}{N_{sample}} \sum_{k=1}^{N_{sample}} \left(\lambda_{mid_{\text{wb}}}(k) - \hat{\lambda}_{mid_{\text{wb}}}(k) \right)^2} \tag{19}$$

where N_{sample} is the number of samples over which the RMSE is evaluated. The RMSE has been computed for each catalyst in two different time windows: the first window spans from 0 to 500 s, where the effects of the intentionally erroneous initialization are more evident, whereas the second window spans from 1500 s to the end of the driving cycle where the OSC estimate is converging to its steady-state value. Results are listed in Table 4. It can also be noted that the RMSE decreases with increasing catalyst age. This result can be explained in terms of signal excitation: as the catalyst degrades, the oxygen buffer is reduced and variations of the normalized exhaust air/fuel ratio are no longer fully attenuated by the catalyst oxygen adsorption/desorption process.

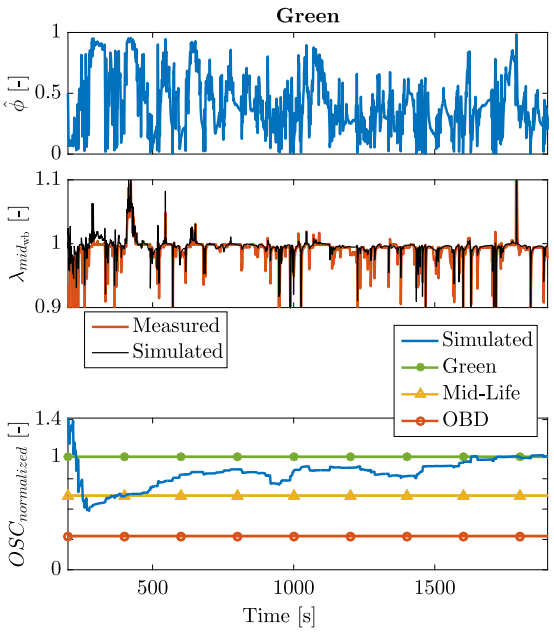

Fig. 9. Simulation results of the estimated and measured $\lambda_{mid_{wb}}$, $\hat{\phi}$ is the average value of oxygen level from all the three spatially discretized cells and $\widehat{OSC}$ is the estimate of oxygen storage capacity (normalized with respect to the OSC of a fresh catalyst) for the Green catalyst.

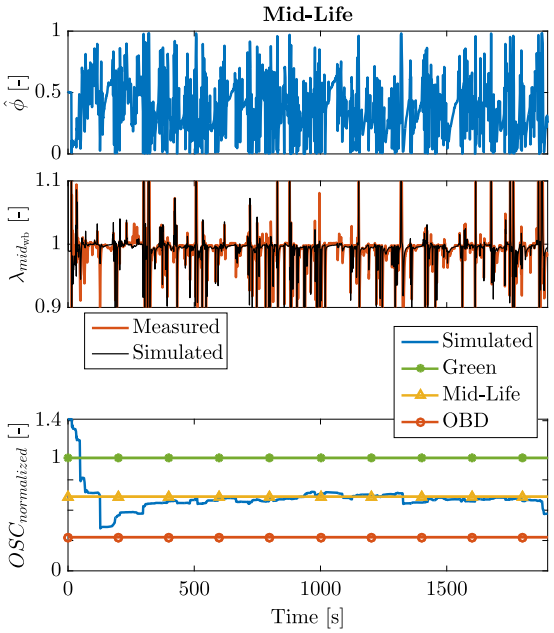

Fig. 10. Simulation results of the estimated and measured $\lambda_{mid_{wb}}$, $\hat{\phi}$ is the average value of oxygen level from all the three spatially discretized cells and $\widehat{OSC}$ is the estimate of oxygen storage capacity (normalized with respect to the OSC of a fresh catalyst) for the Mid-Life catalyst.

Thus, from a system dynamics perspective, the air/fuel ratio located downstream of the catalyst inevitably contains more high-frequency harmonics. As a consequence of a more excited measurement signal, the dEKF improves its estimate and the OSC rate of convergence increases.

In the previous section, the covariance term Q_4 has been used as tuning parameter and its final value will affect the filter performance. Fig. 12(a) shows the OSC estimated trajectories as a function of Q_4.

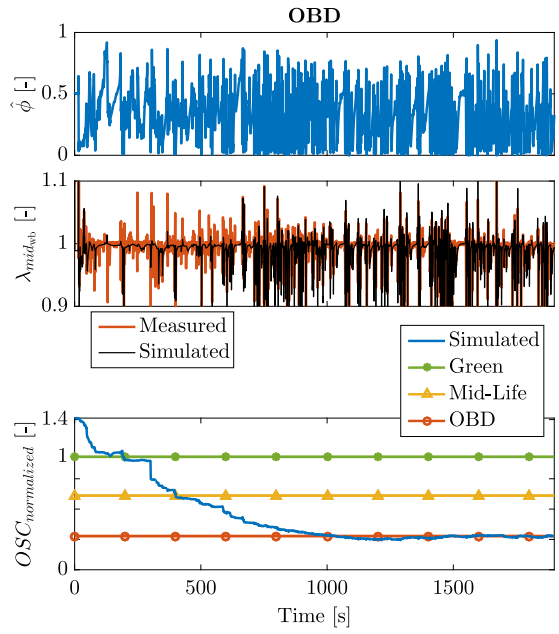

Fig. 11. Simulation results of the estimated and measured $\lambda_{mid_{wb}}$, $\hat{\phi}$ is the average value of oxygen level from all the three spatial discretization cells and $\widehat{OSC}$ is the estimate of oxygen storage capacity (normalized with respect to the OSC of a fresh catalyst) for the OBD catalyst.

Table 4
Post TWC lambda RMSE values evaluated for the aged catalysts. The RMSE has been evaluated in two different time windows in order to quantify the dEKF performance with respect to time. In the first time window, up to 500 s, the catalyst is more influenced by a wrong initial guess of the aging parameter; in the second, after 1500 s, the estimates have settled to their reference values. For all the three aged devices, a good estimate of the aging parameter results in at least 50% improvement in the output tracking performance.

Catalyst	$RMSE$ $(Time < 500\ s)$ [%]	$RMSE$ $(Time > 1500\ s)$ [%]
Green	3.4075	1.5696
Mid-life	4.6733	2.002
OBD	4.8827	1.3932

Large Q_4 values produce expedient convergence, but promote noise at steady state. Low Q_4 values produce less steady state estimate variations but exhibit a slower rate of convergence. A good trade off between acceptable chattering and convergence settling time is found in the range of values $10^{-5} \leq Q_4 \leq 10^{-4}$.

In Fig. 12(b) the convergence settling time and standard deviation of the steady state estimation have been evaluated for different values of Q_4. For values above $Q_4 = 4 \cdot 10^{-5}$ it is possible to obtain a fast OSC convergence, at the price of a larger standard deviation that may not be acceptable for the purposes of the application under study. On the other hand, as OSC is a slow varying variable, a slow settling time is deemed acceptable. For these reasons, a slower solution with less chattering is preferred here. As shown, good performance can be achieved using $Q_4 = 0.2 \cdot 10^{-5}$. For the OBD catalyst, this tuning value requires approximately 1000 s for the estimate to settle.

A study of the OSC estimation with respect to different initial OSC values is finally shown in Fig. 13.

6.2. Observability analysis

The dEKF estimation results are strictly constrained upon having observable model states from measured outputs. Due to the complexity of the system dynamics, this work checks observability on the linearized system. If observability is granted for the linearized case, then the

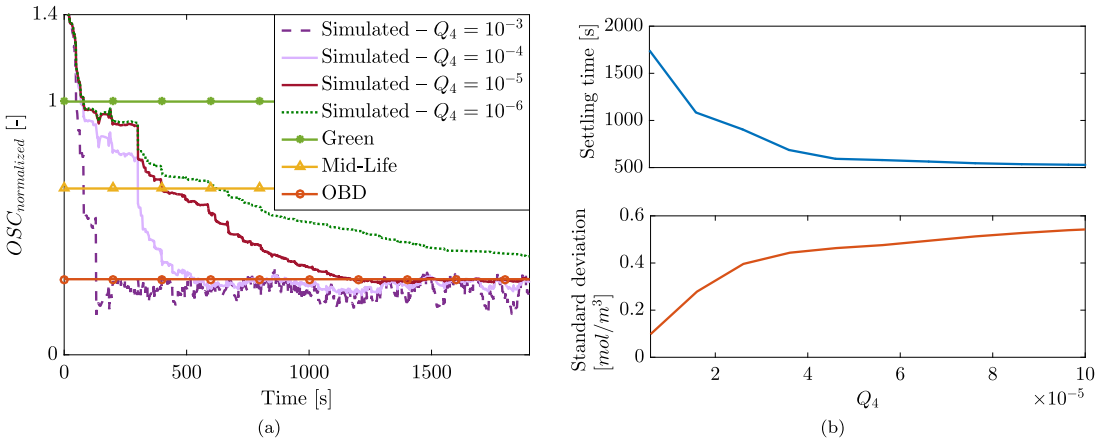

Fig. 12. Figure (a): estimation of OSC – normalized with respect to OSC value from fresh catalyst – for different values of the dEKF tuning parameter Q_4. Figure (b): trade-off comparison of convergence settling time and the estimated OSC's standard deviation at steady-state for a range of Q_4 values.

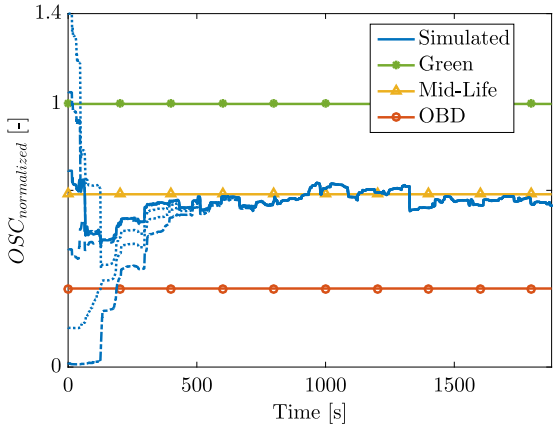

Fig. 13. Estimation of OSC – normalized with respect to the fresh catalyst OSC value – for different initialization values of the observer. The proposed observer exhibits to be robust behavior against different initial conditions, with an initial transient of 700 s.

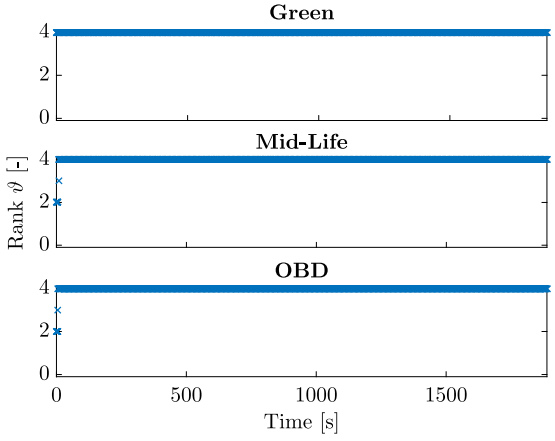

Fig. 14. Rank evaluation of the observability matrix for differently aged catalysts on the FTP driving cycle. Both the Mid-Life and OBD aged catalysts have instances with lack of observability at the beginning of the test. Yet, the performance of the algorithm have proved not to be influenced by those 'isolated' unobservable states.

nonlinear system is locally observable in the neighborhood near the linearization (Vidyasagar, 2002).

The observability matrix is defined for the linearized system as:

$$O(k) = \begin{bmatrix} \hat{C}(k) \\ \hat{C}(k) \cdot \hat{A}(k) \\ \vdots \\ \hat{C}(k) \cdot \hat{A}^{n-1}(k) \end{bmatrix}. \tag{20}$$

where n is equal to 4 and matrices $\hat{A}$ and $\hat{C}$ were defined in Section 5.

The numerical observability matrix ranks for the three aged TWCs are shown in Fig. 14. Except for the initial time instants, for the MID-Life and OBD aged catalysts the matrix rank is always full.

7. Rapid control prototyping

The control strategy to estimate the oxygen storage level and the oxygen storage capacity through the dEKF presented in this work has been validated on a passenger vehicle operating on a four-wheel chassis dynamometer at the Clemson University International Center for Automotive Research. The dEKF was modeled in Simulink and interfaced to the engine control unit (ECU) via an ETAS ES910, providing real-time access to ECU parameters. The exhaust mass flow rate is read out of the vehicle ECU through the GPEC2 port. Simultaneously, pre- and post-TWC temperature and lambda signals were integrated with the model

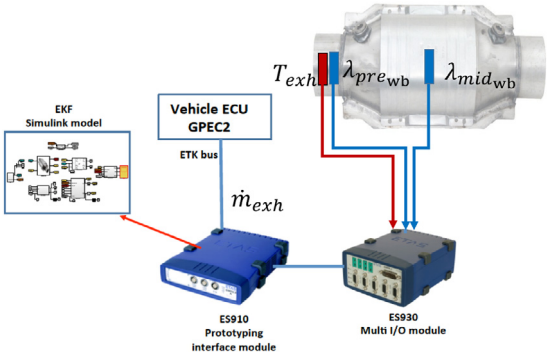

Fig. 15. Rapid test prototyping setup.

via an ETAS ES 930 Multi I/O module. The rapid prototyping scheme implemented in this work is shown in Fig. 15.

For real-time hardware validation, a catalyst with $OSC_{normalized}$ equal to 0.7 was installed on the vehicle. The in-vehicle validation was conducted over the FTP and JAP 15 driving cycles. The initial OSC value was set to that of a green catalyst, representing a full parameter reset during vehicle repair, and to a higher value, to prove convergence as in simulation (see Fig. 16).

Fig. 16. In-vehicle testing to assess the feasibility and performance of the proposed estimator.

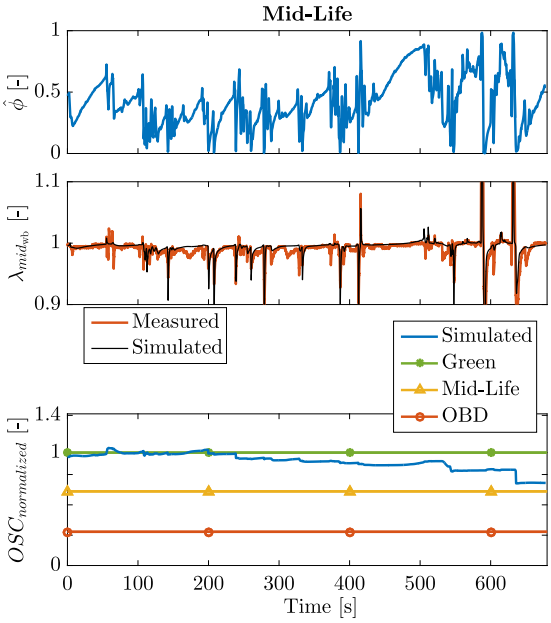

Fig. 17. (top) Experimentally estimated $\hat{\phi}$ (top) - calculated as the average value of oxygen level from the three spatially discretized cells; (mid) experimentally estimated and measured $\lambda_{mid_{wb}}$; (bottom) experimentally estimated $\widehat{OSC}$ (normalized with respect to fresh catalyst OSC) for the Mid-Life catalyst. This test was conducted following the JAP 15 driving cycle.

Table 5
Summary of the RMSE values computed from the JAP 15 and FTP cycles over Mid-Life catalyst used in the rapid control prototyping experiments.

Catalyst	Driving cycle	RMSE [%]
Mid-life	JAP 15	1.69
Mid-life	FTP	1.55
Mid-life	FTP	1.27

As shown in Fig. 17, convergence in parameter estimation is reached in the case of FTP, whereas the shorter duration of JAP 15 hinders the convergence.

To prove the robustness, a different FTP run was performed with different driver (Fig. 18) and different initial conditions for the OSC value (Fig. 19).

Table 5 reports the RMSE values obtained from the rapid control prototyping experiments.

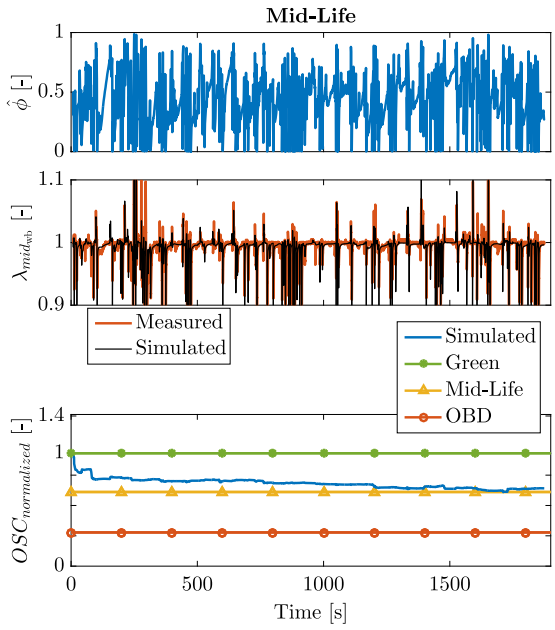

Fig. 18. (top) Experimentally estimated $\hat{\phi}$ (top) - calculated as the average value of oxygen level from the three spatially discretized cells; (mid) experimentally estimated and measured $\lambda_{mid_{wb}}$; (bottom) experimentally estimated $\widehat{OSC}$ (normalized with respect to fresh catalyst OSC) for the Mid-Life catalyst. This test was conducted following the FTP driving cycle.

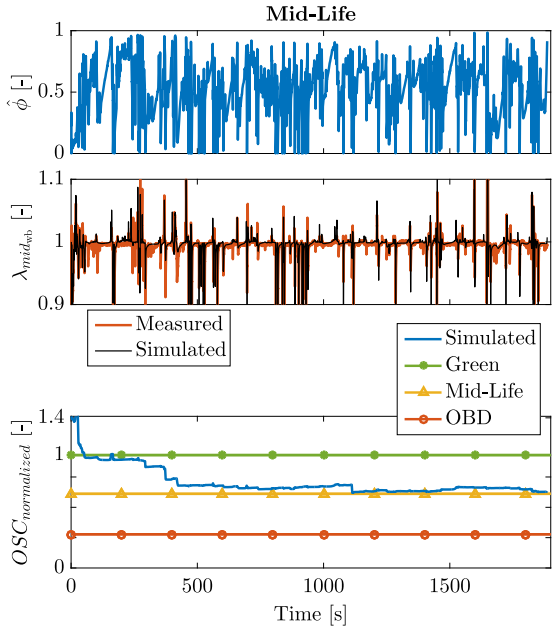

Fig. 19. (top) Experimentally estimated $\hat{\phi}$ (top) - calculated as the average value of oxygen level from the three spatially discretized cells; (mid) experimentally estimated and measured $\lambda_{mid_{wb}}$; (bottom) experimentally estimated $\widehat{OSC}$ (normalized with respect to fresh catalyst OSC) for the Mid-Life catalyst. This test was conducted following the FTP driving cycle.

8. Conclusions

In this work, we first assessed how different TWC lambda sensor technologies can affect the ability to monitor the TWC health, and then we designed a dEKF for the purpose of estimating the actual oxygen storage and oxygen capacity during vehicle operation.

Using a PDE model of the TWC, the performance of a wide band lambda sensor was compared against different switch-type sensors – used downstream of the TWC – in their ability to facilitate OSC estimation. A Fisher information analysis was employed to quantify the uncertainty of the estimated OSC for the various lambda sensors. it is shown that a wide band lambda sensor leads to limited uncertainty in the OSC estimation as opposed to switch-type lambda sensors, which instead produce measurements that do not contain enough information for the aging parameter to be identified.

Wide band lambda sensors are then used in the development of dEKF. The observer was developed from a physics-based 1-D TWC model derived in previous works by the authors. The dEKF was designed to estimate, in real-time, the catalyst oxygen storage level, ϕ, and the age dependent oxygen storage capacity OSC. Simulation results, validated against transient experimental measurements, proved the ability of the observer to estimate the aging parameter, OSC, for different catalysts. The accurate online OSC estimation reduces the RMSE of predicted post TWC lambda signal response, aiding any control design which utilizes disparities between measured and predicted post TWC lambda for air-to-fuel ratio alterations.

Declaration of competing interest

The authors declare that they have no known competing financial interests or personal relationships that could have appeared to influence the work reported in this paper.

Acknowledgments

The authors greatly acknowledge the technical and financial support from FCA US LLC (Auburn Hills, MI 48326 USA), and the National Science Foundation, US through the CAREER Award number CMMI-1839050, under which this work was conducted.

References

Anguelova, M. (2007). *Observability and identifiability of nonlinear systems with applications in biology* (Ph.D. thesis), Chalmers University of Technology Gothenburg, Sweden.

Auckenthaler, T. S. (2005). *Modelling and control of three-way catalytic converters* (Ph.D. thesis), ETH Zürich.

Auckenthaler, T. S., Onder, C. H., & Geering, H. P. (2004). *Online estimation of the oxygen storage level of a three-way catalyst*: *SAE technical paper 2004-01-0525*, http://dx.doi.org/10.4271/2004-01-0525.

Auto accessories garage. (2020). www.autoaccessoriesgarage.com.

Balenovic, M. (2002). *Modelling and model-based control of a three-way catalytic converter* (Ph.D. thesis), University of Eindhoven.

Balenovic, M., Backx, T., & de Bie, T. (2002). *Development of a model-based controller for a three-way catalytic converter*: *SAE technical paper 2002-01-0475*, http://dx.doi.org/10.4271/2002-01-0475.

Balenovic, M., Backx, A. C. P. M., & Hoebink, J. H. B. J. (2001). *On a model-based control of a three-way catalytic converter*: *SAE technical paper 2001-01-0937*, http://dx.doi.org/10.4271/2001-01-0937.

Bekiaris-Liberis, N., Jankovic, M., & Krstic, M. (2012). PDE-Based analysis and control of the oxygen storage level in three-way catalytic converters. In *Proceedings of the conference on decision and control (CDC)*. http://dx.doi.org/10.1109/CDC.2012.6426283.

Bellman, R., & Åström, K. J. (1970). On structural identifiability. *Mathematical Biosciences*, http://dx.doi.org/10.1016/0025-5564(70)90132-X.

Bosch (2021). Lambda sensor LSU 4.9 datasheet. https://aviorace.it/wp-content/uploads/2021/01/Bosch-LSU49_e.pdf.

Brandt, E. P., Wang, Y., & Grizzle, J. W. (2000). Dynamic modeling of a three-way catalyst for SI engine exhaust emission control. *IEEE Transactions on Control Systems Technology*, http://dx.doi.org/10.1109/87.865850.

Cooper, B. J. (1983). Durability of platinum-containing automotive exhaust control catalysts. *Platinum Metals Review*.

DE Solutions, I., & Tecogen, I. (2011). Engine CHP emission control technology, final project report. *California Energy Commission*.

Depcik, C., & Assanis, D. (2005). One-dimensional automotive catalyst modeling. *Progress in Energy and Combustion Science*, http://dx.doi.org/10.1016/j.pecs.2005.08.001.

Dettu, F., & Onori, S. (2021). On rigorous model-order reduction of the thermal and oxygen storage dynamics of three way catalytic converters. *Transactions of the ASME. Journal of Dynamic Systems, Measurement and Control*, *143*.

Dieselnet website. (2020). www.dieselnet.com/tech/images/diesel/exh/sys/~mb_a.jpg.

Dynamometer drive schedules. (2020). https://www.epa.gov/vehicle-and-fuel-emissions-testing/dynamometer-drive-schedules.

EPA - history of reducing air pollution from transportation in the United States (U.S.). (2020). www.epa.gov/air-pollution-transportation/accomplishments-and-success-air-pollution-transportation.

Fathy, H., & Sharma, A. (2014). Fisher Identifiability analysis for a periodically-excited equivalent-circuit lithium-ion battery model. In *2014 American control conference*. http://dx.doi.org/10.1109/ACC.2014.6859360.

Gandhi, H. S., Piken, A. G., Shelef, M., & Delosh, R. (1976). *Laboratory evaluation of three-way catalysts*: *SAE technical paper 760201*, http://dx.doi.org/10.4271/760201.

Gelmini, S., Sabatini, S., Hoffman, M. A., & Onori, S. (2017). Development and experimental validation of a dual extended kalman filter for three way catalytic converter. In *Proceedings of the American control conference (ACC)*. http://dx.doi.org/10.23919/ACC.2017.7963792.

Godi, R., & Onori, S. (2017). Reduced order model design for three way catalytic converters. In *1st IEEE conference on control technology and applications*. http://dx.doi.org/10.1109/CCTA.2017.8062571.

González-Velasco, J. R., Botas, J. A., Ferret, R., González-Marcos, M. P., Marc, J. L., & Gutiérrez-Ortiz, M. A. (2000). Thermal aging of Pd/Pt/Rh automotive catalysts under a cycled oxidizing–reducing environment. *Catalysis Today*, http://dx.doi.org/10.1016/S0920-5861(00)00304-7.

Grewal, M. S. (2020). *Kalman filtering*. Springer, http://dx.doi.org/10.1002/9781119547860.ch10.

Hermann, R., & Krener, A. J. (1977). Nonlinear controllability and observability. *IEEE Transactions on Automatic Control*, http://dx.doi.org/10.1109/TAC.1977.1101601.

Heywood, J. B. (1988). *Internal combustion engine fundamentals*. Mcgraw-hill.

IPPC (2014). Climate change 2014: Mitigation of climate change. www.ipcc.ch/report/ar5/wg3/.

Jones, J. C. P., Roberts, J. B., Bernard, P., & Jackson, R. A. (2000). *A simplified model for the dynamics of a three-way catalytic converter*: *SAE technical paper 2000-01-0652*, http://dx.doi.org/10.4271/2000-01-0652.

Kim, G. (1982). Ceria-promoted three-way catalysts for auto exhaust emission control. *Industrial & Engineering Chemistry Product Research and Development*, http://dx.doi.org/10.1021/i300006a014.

Kiwitz, P., Onder, C., & Guzzella, L. (2012). Control-oriented modeling of a three-way catalytic converter with observation of the relative oxygen level profile. *Journal of Process Control*, http://dx.doi.org/10.1016/j.jprocont.2012.04.014.

Kumar, P., Makki, I., & Filev, D. (2014). A non-intrusive three-way catalyst diagnostics monitor based on support vector machines. In *2014 IEEE international conference on systems, man, and cybernetics*. http://dx.doi.org/10.1109/SMC.2014.6974149.

Ljung, L. (1998). *System identification*. Springer.

Magni, L., & Scattolini, R. (2014). *Advanced and multivariable control*. Pitagora.

Matam, S. K., Otal, E. H., Aguirre, M., Winkler, A., Ulrich, A., Rentsch, D., et al. (2012). Thermal and chemical aging of model three-way catalyst Pd/Al 2 O 3 and its impact on the conversion of CNG vehicle exhaust. *Catalysis Today*, http://dx.doi.org/10.1016/j.cattod.2011.09.030.

Moldovan, M., Rauch, S., Morrison, G. M., Gomez, M., & Antonia Palacios, M. (2003). Impact of ageing on the distribution of platinum group elements and catalyst poisoning elements in automobile catalysts. *Surface and Interface Analysis*, http://dx.doi.org/10.1002/sia.1541.

Montenegro, G., & Onorati, A. (2009). *1D thermo-fluid dynamic modeling of reacting flows inside three-way catalytic converters*: *SAE technical paper 2009-01-1510*, http://dx.doi.org/10.4271/2009-01-1510.

Mopar part 05149180 AA datasheet. (2020). https://www.factorychryslerparts.com/.

Muske, K. R., & Jones, J. C. P. (2004). Estimating the oxygen storage level of a three-way automotive catalyst. In *Proceedings of American control conference, 2004*. http://dx.doi.org/10.23919/ACC.2004.1383944.

Nesbit, M., Fergusson, M., Colsa, A., Ohlendorf, J., Hayes, C., Paquel, K., et al. (2016). Comparative study on the differences between the EU and US legislation on emissions in the automotive sector. European Parlament - Directorate General for Internal Policies.

Ngo, C., Koenig, D., Sename, O., & Béchart, H. (2013). A reduced model of three ways catalyst converter and stored oxygen rate estimation using switched observer. In *12th biannual European control conference*. ECC 2013, http://dx.doi.org/10.23919/ECC.2013.6669754.

Norton, J. P. (2009). *An introduction to identification*. Courier Corporation.

Oh, S. H., & Cavendish, J. C. (1982). Transients of monolithic catalytic converters. Response to step changes in feedstream temperature as related to controlling automobile emissions. *Industrial & Engineering Chemistry Product Research and Development*, http://dx.doi.org/10.1021/i300005a006.

Sabatini, S., Gelmini, S., Hoffman, M. A., & Onori, S. (2017). Design and experimental validation of a physics-based oxygen storage - thermal model for three way catalyst including aging. *Control Engineering Practice*, *68*, 89–101. http://dx.doi.org/10.1016/j.conengprac.2017.07.007.

Sabatini, S., Kil, I., Dekar, J., Hamilton, T., Wuttke, J., Smith, M. A., et al. (2015). A new semi-empirical temperature model for the three way catalytic converter. *IFAC-PapersOnLine*, *48*(15), 434–440. http://dx.doi.org/10.1016/j.ifacol.2015.10.062.

Sabatini, S., Kil, I., Hamilton, T., Wuttke, J., Del Rio, L., Smith, M., et al. (2016). *Characterization of aging effect on three-way catalyst oxygen storage dynamics*: *SAE technical paper 2016-01-0971*, http://dx.doi.org/10.4271/2016-01-0971.

Santillo, M., Magner, S., Uhrich, M., & Jankovic, M. (2015). Towards ECU-executable control-oriented models of a three-way catalytic converter. *Proceedings of the ASME DSCC2015-9653*, http://dx.doi.org/10.1115/DSCC2015-9653.

Schallock, R. W., Muske, K. R., & Jones, J. C. P. (2009). *Model predictive functional control for an automotive three-way catalyst*: *SAE technical paper 2009-01-0728*, http://dx.doi.org/10.4271/2009-01-0728.

Schmidt, A. P., Bitzer, M., Imre, A. W., & Guzzella, L. (2010). Experiment-driven electrochemical modeling and systematic parameterization for a lithium-ion battery cell. *Journal of Power Sources*, http://dx.doi.org/10.1016/j.jpowsour.2010.02.029.

Shamim, T., Shen, H., Sengupta, S., Son, S., & Adamczyk, A. A. (2002). A comprehensive model to predict three-way catalytic converter performance. *Journal of Engineering for Gas Turbines and Power*, http://dx.doi.org/10.1115/1.1424295.

Sharma, A., & Fathy, H. K. (2014). Fisher identifiability analysis for a periodically-excited equivalent-circuit lithium-ion battery model. In *Proceedings of the American control conference (ACC)*. http://dx.doi.org/10.1109/ACC.2014.6859360.

Tomforde, M., Drewelow, W., Duenow, P., Lampe, B., & Schultalbers, M. (2013). *A post-catalyst control strategy based on oxygen storage dynamics*: *SAE technical paper 2013-01-0352*, http://dx.doi.org/10.4271/2013-01-0352.

Utz, T., Fleck, C., Frauhammer, J., Seiler-Thull, D., & Kugi, A. (2014). Extended Kalman filter and adaptive backstepping for mean temperature control of a three-way catalytic converter. *International Journal of Robust and Nonlinear Control*, http://dx.doi.org/10.1002/rnc.3065.

Vajda, S., Rabitz, H., Walter, E., & Lecourtier, Y. (1989). Qualitative and quantitative identifiability analysis of nonlinear chemical kinetic models. *Chemical Engineering Communications*, http://dx.doi.org/10.1080/00986448908940662.

Vidyasagar, M. (2002). *Nonlinear systems analysis*. Siam.